Conditions for use and implementation of globally-aligned versus local baseplate coordinate systems when computing migration using radiostereometric analysis

Niesen, A.E.; Kaptein, B.L.; Hull, M.L.

Conditions for Use and Implementation of Globally-Aligned Versus Local Baseplate Coordinate Systems When Computing Migration Using Radiostereometric Analysis

Abigail E. Niesen
Department of Biomedical Engineering,
University of California,
Davis One Shields Avenue,
Davis, CA 95616
e-mail: abniesen@ucdavis.edu

Bart L. Kaptein
Department of Orthopaedic Surgery,
Leiden University Medical Center,
P.O. Box 9600,
Leiden 2300 RC, The Netherlands
e-mail: b.l.kaptein@lumc.nl

Maury L. Hull
Department of Biomedical Engineering,
University of California,
Davis One Shields Avenue,
Davis, CA 95616;
Department of Mechanical Engineering,
University of California,
Davis One Shields Avenue,
Davis, CA 95616;
Department of Orthopaedic Surgery,
University of California Davis Medical Center,
4860 Y Street, Suite 3800,
Sacramento, CA 95817
e-mail: mlhull@ucdavis.edu

Radiostereometric analysis can be used for computing movement of a tibial baseplate relative to the tibia (termed migration) to determine stability of fixation. Quantifying migration in six degrees of freedom requires establishing a coordinate system in which to express the movement. Establishing consistent migration directions among patients and baseplate designs remains challenging. Deviations in imaging alignment (tibia/baseplate alignment during image acquisition) and surgical alignment (baseplate alignment on tibia) will affect computed migrations when using the conventional globally-aligned baseplate coordinate system (BCS) (defined by calibration box). Computing migration using a local BCS (defined by baseplate) may be preferrable. This paper (1) summarizes the migration equations when using a globally-aligned versus local BCS, (2) proposes a method for defining a local BCS, and (3) demonstrates differences in the two BCSs for an example patient whose baseplate has rotational deviations due to imaging or surgical alignments. Differences in migration for the two BCSs ranged from about ±0.5 mm in translations and −0.4 deg to 0.7 deg in rotations. Differences were largest for deviations in internal-external rotation and smallest for deviations in varus-valgus rotation. An example demonstrated that the globally-aligned BCS resulted in migration being quantified as subsidence instead of liftoff, thereby changing fundamental interpretations. Because migrations computed using a local BCS are independent of imaging and surgical alignments and instead characterize migration using baseplate features, a local BCS enhances consistency in migration directions among patients and baseplate designs relative to the interface in which fixation may be compromised. [DOI: 10.1115/1.4056802]

Keywords: relative movement, six degrees of freedom movement, anatomic directions, biplanar images, implant stability

Introduction

Quantifying migration of tibial baseplates is important to determine stability of fixation [1–3]. Migration is the relative movement between the baseplate and underlying tibia bone and can be measured using radiostereometric analysis (RSA) which requires obtaining two pairs of radiographs [4,5]. The first pair of radiographs is acquired immediately postoperatively to provide a baseline for the migration computation and the second pair is acquired at a follow-up time point [5]. The baseline defines the reference position of the baseplate relative to the tibia using markers placed in the bone [4]. To determine migration between the two pairs of radiographs, two successive registrations are performed. The first registration aligns the tibia markers in the second pair of radiographs with the tibia markers in the first pair of radiographs [4]. This first registration removes any difference in patient positioning between the reference pair of radiographs and the follow-up pair of radiographs [4]. The second registration aligns the baseplate in the second pair of radiographs with the baseplate in the first pair [4]. The difference between the second and first registrations quantifies baseplate migration [4].

Quantifying migration requires establishing a coordinate system in which to express the relative movement of the baseplate between the baseline and follow-up pairs of radiographs. For RSA, radiograph acquisition occurs in the presence of a calibration box which contains markers at known locations thereby forming a global coordinate system (GCS) [4,5]. The GCS is necessary to determine the respective locations of the baseplate and tibia in three-dimensional (3D) from each pair of radiographs using projective geometry [4]. Once the baseplate and tibia are located in 3D, the migration computation is generally performed using a globally-aligned baseplate coordinate system (BCS) where the axes directions are aligned with the GCS and the origin is located at the centroid of the baseplate (or insert) markers (Fig. 1(*a*)) [4].

Measuring migration using the globally-aligned BCS requires imaging alignment, a condition in which the X-ray technician positions the patient such that the GCS axes correspond to anatomic tibial directions where $X = x_{GA}$ (medial positive), $Y = y_{GA}$ (proximal positive), and $Z = z_{GA}$ (anterior positive) (i.e., right-handed coordinate system for right knee) (Fig. 1(*a*)) [5] during radiograph acquisition. However, satisfying the condition of imaging alignment is challenging. For example, misalignments in internal-external rotation up to 15 deg may occur [6] (Table 1). Furthermore, reorienting the patient's limb during image acquisition can increase accuracy for model-based RSA by creating a contour with more details when registering the 3D model onto the

Manuscript received September 10, 2022; final manuscript received January 24, 2023; published online March 8, 2023. Assoc. Editor: Matty J. Major.

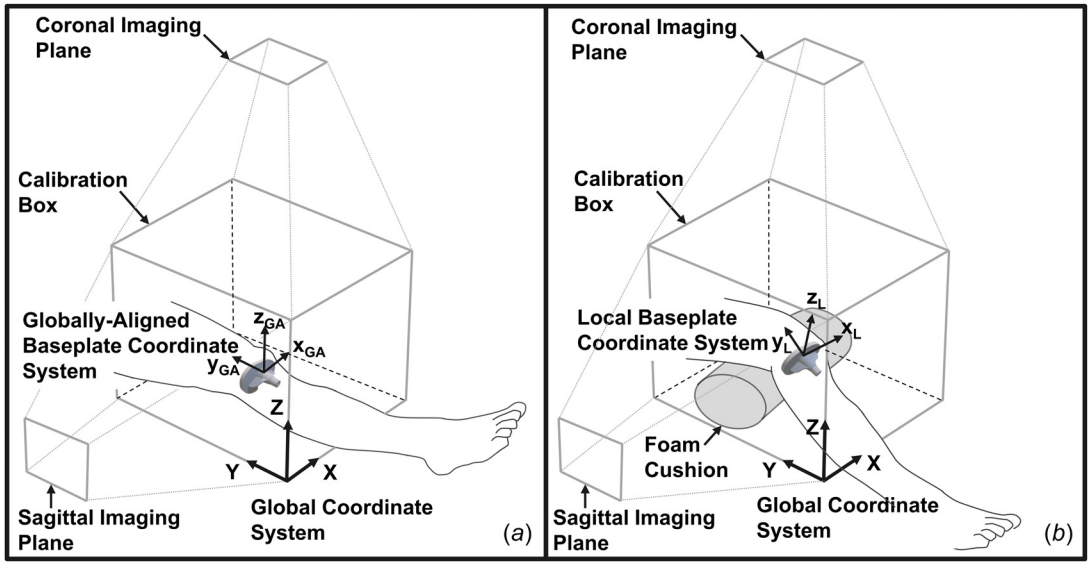

Fig. 1 (*a*) **Globally-aligned baseplate coordinate system (BCS) with axes parallel to those of the global coordinate system (GCS) but with origin located at the baseplate centroid. Patient must be positioned such that the GCS axes correspond to anatomic tibial directions where $X = x_{GA}$ (medial positive), $Y = y_{GA}$ (proximal positive), and $Z = z_{GA}$ (anterior positive) to obtain clinically relevant migrations. (*b*) Local BCS (defined by features on the baseplate) in which clinically relevant migrations are independent of patient positioning.**

radiographs [7]. As such, researchers may choose to purposefully not satisfy the condition of imaging alignment by reorienting the patient's limb relative to the geometry of the calibration box, in which case computing migration using the globally-aligned BCS will result in anatomical errors in the six degrees of freedom. These anatomical errors occur because the GCS axes no longer correspond to anatomic directions when the condition of imaging alignment is not satisfied; therefore, interpretation of the migration direction is incorrect.

Furthermore, even when the condition of imaging alignment is met, there exists another condition, termed surgical alignment (i.e., alignment of the baseplate relative to the tibial mechanical axis), which must be satisfied to obtain migrations relative to the baseplate-tibia interface. Surgical alignment is not met for patients who receive a total knee replacement (TKR) using kinematic alignment [8] since baseplates may be positioned up to 10 deg varus [9] and/or with 17 deg posterior slope [10] to match the native tibial plateau (Table 1). Patients who receive TKR using mechanical alignment satisfy surgical alignment in the coronal plane if the baseplate is perpendicular to the tibial mechanical axis, but do not satisfy surgical alignment in the sagittal plane since the baseplate is positioned with a posterior slope of 3 deg to 7 deg [15]. Also, when the tibial baseplate is misaligned on the tibia, particularly in internal-external rotation, surgical alignment is not satisfied. Clinically relevant ranges of rotational deviations in imaging alignment and/or surgical alignment are summarized (Table 1).

When deviations in imaging alignment and/or surgical alignment are of sufficient magnitude to affect interpretations of migration, an alternative coordinate system must be used for computing

Table 1 Instances in which deviations from the two conditions of imaging alignment and surgical alignment may occur. Clinically relevant ranges of rotational deviations in baseplate alignment relative to the imaging planes are indicated.

	Imaging alignment	Surgical alignment	
	Baseplate alignment during imaging	Baseplate alignment relative to tibial mechanical axis for mechanical alignment	Baseplate alignment relative to tibial mechanical axis for kinematic alignment
Flexion-extension (FE) rotation	Baseplate is rotated in FE relative to imaging planes Range: 0 deg to 25 deg flexion [7]	Target: restore average posterior slope Range: 3 deg to 7 deg posterior slope [15]	Target: restore posterior slope (i.e., FE rotation) to native Range: 17 deg posterior slope to 10 deg anterior slope [10]
Internal-external (IE) rotation	Baseplate is rotated in IE relative to imaging planes Range: 15 deg internal to 15 deg external [6]	Target: various (e.g., medial 1/3 of tibial tubercle-PCL, medial border of tibial tubercle-PCL, etc.) Range: 44 deg internal to 46 deg external [16]	Target: baseplate aligned with FE axis of femur Range: 10 deg internal to 14 deg external [22]
Varus-valgus (VV) rotation	Baseplate is rotated in VV relative to imaging planes Range: 5 deg valgus to 5 deg varus [6]	Target: baseplate perpendicular to mechanical axis within 3 deg (i.e., 0 deg VV rotation) Range: 3 deg valgus to 4 deg varus [23]	Target: restore VV to native Range: 0 deg to 10 deg varus [9]

migration. A logical alternative proposed herein is a local BCS whose axes and origin are defined by features on the baseplate. Because a local BCS is defined by the features on the baseplate, the above conditions do not have to be satisfied to produce anatomically relevant migrations (Fig. 1(*b*)). For consistency in model-based-RSA, a local BCS can be defined by the 3D model allowing standardization between patients. Local BCSs have also been proposed for marker-based RSA and results of an in vitro study showed no reduction in precision compared to using a globally-aligned BCS [6].

Since no prior publication thoroughly explains the conditions for use of a globally-aligned BCS versus a local BCS and their implementation, the objectives of this paper were to (1) summarize the migration equations using the globally-aligned BCS and local BCS, (2) propose a method for defining a local BCS using an example baseplate, and (3) provide a clinical example to demonstrate differences in the two BCSs for a patient whose baseplate has rotational deviations relative to the imaging planes due to imaging or surgical alignment.

Methods

Globally-Aligned Baseplate Coordinate System. Let the tibia be denoted T and the baseplate be denoted B. The position of these two objects in the GCS as determined from their radiograph pairs will be denoted using subscripts "ref" for reference and "fu" for follow-up.

The position vectors for all reference points are summarized in a $3 \times n$ matrix, $\boldsymbol{T}_{ref} = [\boldsymbol{t}_{ref,1} \ldots \boldsymbol{t}_{ref,n}]$, and a $3 \times m$ matrix, $\boldsymbol{B}_{ref} = [\boldsymbol{b}_{ref,1} \ldots \boldsymbol{b}_{ref,m}]$, where n and m are the number of points on the tibia and baseplate, respectively (Fig. 2). The position vectors for all follow-up points are summarized in another $3 \times n$ matrix, $\boldsymbol{T}_{fu} = [\boldsymbol{t}_{fu,1} \ldots \boldsymbol{t}_{fu,n}]$, and another $3 \times m$ matrix, $\boldsymbol{B}_{fu} = [\boldsymbol{b}_{fu,1} \ldots \boldsymbol{b}_{fu,m}]$, (Fig. 2).

Absolute movement of the tibia is defined by $\boldsymbol{R}_T$ and $\boldsymbol{D}_T$ (Fig. 3) and the absolute movement of the baseplate is defined by $\boldsymbol{R}_B$ and $\boldsymbol{D}_B$ as follows [11]

$$\boldsymbol{T}_{fu} = \boldsymbol{R}_T * \boldsymbol{T}_{ref} + \boldsymbol{D}_T * \text{ones} \tag{1}$$

$$\boldsymbol{B}_{fu} = \boldsymbol{R}_B * \boldsymbol{B}_{ref} + \boldsymbol{D}_B * \text{ones} \tag{2}$$

where $\boldsymbol{R}_T$ and $\boldsymbol{R}_B$ are the rotation matrices for the tibia and baseplate, respectively, $\boldsymbol{D}_T$ and $\boldsymbol{D}_B$ are the displacement vectors for the tibia and baseplate, respectively, and ones are a $1 \times n$ matrix and a $1 \times m$ matrix consisting of ones for the tibia and baseplate, respectively.

The tibia point vectors in $\boldsymbol{T}_{ref}$ and $\boldsymbol{T}_{fu}$ are denoted $\boldsymbol{t}_{ref,i}$ and $\boldsymbol{t}_{fu,i}$ for i = 1 to n. Determination of $\boldsymbol{R}_T$ and $\boldsymbol{D}_T$ is performed by solving the orthogonal Procrustes problem for rigid body movement where the following expression is minimized [12,13]

$$\min \sum_{i=1}^{n} (\boldsymbol{R}_T \cdot \boldsymbol{t}_{ref,i} + \boldsymbol{D}_T - \boldsymbol{t}_{fu,i})^2 \tag{3}$$

First, the respective centroid vectors are denoted $\boldsymbol{t}_{ref,c}$ and $\boldsymbol{t}_{fu,c}$ and computed as [12,13]

$$\boldsymbol{t}_{ref,c} = \frac{1}{n} \sum_{i=1}^{n} \boldsymbol{t}_{ref,i} \tag{4}$$

$$\boldsymbol{t}_{fu,c} = \frac{1}{n} \sum_{i=1}^{n} \boldsymbol{t}_{fu,i} \tag{5}$$

Second, the tibia points are translated such that the centroid is at the origin of the GCS [12,13]

$$\boldsymbol{T}_{ref,translated} = [\boldsymbol{t}_{ref,1} - \boldsymbol{t}_{ref,c}, \ldots, \boldsymbol{t}_{ref,n} - \boldsymbol{t}_{ref,c}] \tag{6}$$

$$\boldsymbol{T}_{fu,translated} = [\boldsymbol{t}_{fu,1} - \boldsymbol{t}_{fu,c}, \ldots, \boldsymbol{t}_{fu,n} - \boldsymbol{t}_{fu,c}] \tag{7}$$

Matrix, $\boldsymbol{C}$, is defined as [12,13]

$$\boldsymbol{C} = \boldsymbol{T}_{fu,translated} \cdot \boldsymbol{T}_{ref,translated}^{T} \tag{8}$$

The singular value decomposition of $\boldsymbol{C}$ is computed as [12,13]

$$\boldsymbol{C} = \boldsymbol{U} \cdot \boldsymbol{\Sigma} \cdot \boldsymbol{V}^T \tag{9}$$

The rotation matrix, $\boldsymbol{R}_T$, is computed as [12,13]

$$\boldsymbol{R}_T = \boldsymbol{U} \cdot \text{diag}\left(1, 1, \det(\boldsymbol{U}\boldsymbol{V}^T)\right) \cdot \boldsymbol{V}^T \tag{10}$$

The displacement vector, $\boldsymbol{D}_T$, is computed as [12,13]

$$\boldsymbol{D}_T = \boldsymbol{t}_{fu,c} - \boldsymbol{R}_T \cdot \boldsymbol{t}_{ref,c} \tag{11}$$

Equations (3)–(11) can be repeated to determine $\boldsymbol{R}_B$ and $\boldsymbol{D}_B$ for the baseplate.

To simplify the remaining mathematical equations, the rotation matrix, $\boldsymbol{R}_T$, and displacement vector, $\boldsymbol{D}_T$, are combined into a 4×4 transformation matrix $\boldsymbol{T}_T$, (i.e., homogeneous transformation

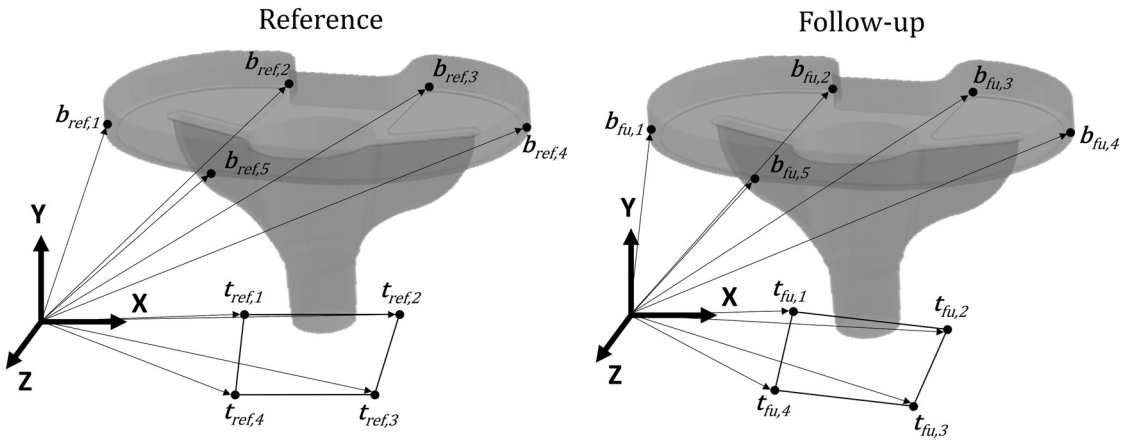

Fig. 2 Illustration of five baseplate points ($\boldsymbol{b}_{ref,1} \ldots \boldsymbol{b}_{ref,5}$ summarized as $\boldsymbol{B}_{ref}$ and $\boldsymbol{b}_{fu,1} \ldots \boldsymbol{b}_{fu,5}$ summarized as $\boldsymbol{B}_{fu}$) and four tibia points ($\boldsymbol{t}_{ref,1} \ldots \boldsymbol{t}_{ref,4}$ summarized as $\boldsymbol{T}_{ref}$ and $\boldsymbol{t}_{fu,1} \ldots \boldsymbol{t}_{fu,4}$ summarized as $\boldsymbol{T}_{fu}$) in the global coordinate system. View of baseplate is from an anterior superior perspective.

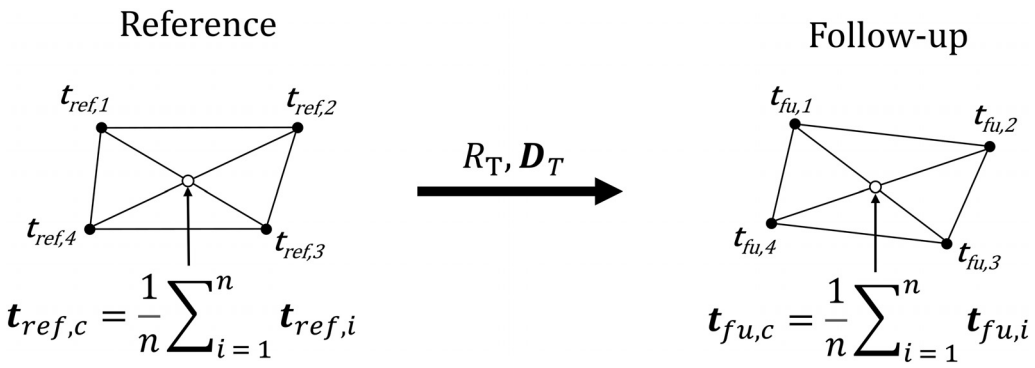

Fig. 3 Illustration of the absolute movement of T_{ref} to T_{fu} by rotation, R_T, and displacement, D_T. The open circles indicate the centroids, $t_{ref,c}$ and $t_{fu,c}$, respectively.

coordinates [14]) which describes the absolute movement of the tibia.

$$\boldsymbol{T}_T = \begin{bmatrix} \boldsymbol{R}_T & \boldsymbol{D}_T \\ 0^T & 1 \end{bmatrix}$$

Similarly, $\boldsymbol{R}_B$ and $\boldsymbol{D}_B$ also are combined into a 4×4 transformation matrix, $\boldsymbol{T}_B$, which describes the absolute movement of the baseplate.

$$\boldsymbol{T}_B = \begin{bmatrix} \boldsymbol{R}_B & \boldsymbol{D}_B \\ 0^T & 1 \end{bmatrix}$$

For readers not familiar with homogeneous coordinates, mathematical equations using Cartesian coordinates are provided in the Appendix.

To compute the relative transformation, the two absolute transformations are combined in Eq. (12), where the second term is the absolute transformation of the baseplate, and the first term applies the inverse of the absolute transformation of the tibia markers to the absolute transformation of the baseplate

$$\boldsymbol{T}^0_{\text{rel}} = \boldsymbol{T}_T^{-1} \cdot \boldsymbol{T}_B \tag{12}$$

$\boldsymbol{T}^0_{\text{rel}}$ is a 4×4 transformation matrix which can be decomposed into the relative rotation matrix, $\boldsymbol{R}^0_{\text{rel}}$ (i.e., the rotation component of migration), and relative displacement vector, $\boldsymbol{D}^0_{\text{rel}}$ (i.e., the displacement component of migration) of the baseplate relative to the tibia

$$\boldsymbol{T}^0_{\text{rel}} = \begin{bmatrix} \boldsymbol{R}^0_{\text{rel}} & \boldsymbol{D}^0_{\text{rel}} \\ 0^T & 1 \end{bmatrix}$$

This transformation describes the rotation matrix and displacement vector defined with respect to the GCS (defined by the calibration box in the reference pair of radiographs and indicated by the superscripted zero). As a result, the translation component of $\boldsymbol{T}^0_{\text{rel}}$ is the translation using the origin of the GCS, resulting in a clinically irrelevant displacement vector, $\boldsymbol{D}^0_{\text{rel}}$, because the origin of the GCS is outside the baseplate. For a clinically relevant displacement, it is important to compute the transformation, $\boldsymbol{T}^0_{\text{rel}}$, using a coordinate system having its origin in a point on the baseplate. Thus, a vector, $\boldsymbol{b}_0$, describes the transformation of the GCS origin to a point on the baseplate. The resulting coordinate system is a globally-aligned BCS, where the axes directions are aligned with the GCS and the origin is located on the baseplate. Conventionally, the origin of the globally-aligned BCS is the centroid of the baseplate markers (attached to the implant or inserted within the polyethylene) for marker-based RSA or the centroid of all points on the 3D model for model-based RSA. To calculate the relative movement using the globally-aligned BCS, termed $\boldsymbol{T}^{\text{b0}}_{\text{rel}}$, an extra transformation, $\boldsymbol{T}_{\text{b0}}$, is used where $\boldsymbol{T}_{\text{b0}}$ is a 4×4 transformation matrix composed of the identity rotation matrix (i.e., no rotation) and the displacement vector $\boldsymbol{b}_0$

$$\boldsymbol{T}_{\text{b0}} = \begin{bmatrix} \boldsymbol{I} & \boldsymbol{b}_0 \\ 0^T & 1 \end{bmatrix}$$

Transformations of the absolute movements $\boldsymbol{T}_T$ and $\boldsymbol{T}_B$ using the point of rotation at $\boldsymbol{b}_0$ are

$$\boldsymbol{T}^{\text{b0}}_T = \boldsymbol{T}_T \cdot \boldsymbol{T}_{\text{b0}} \tag{13}$$

$$\boldsymbol{T}^{\text{b0}}_B = \boldsymbol{T}_B \cdot \boldsymbol{T}_{\text{b0}} \tag{14}$$

For relative movement about $\boldsymbol{b}_0$, substitute Eqs. (13)–(14) into Eq. (12) and simplify

$$\begin{aligned} \boldsymbol{T}^{\text{b0}}_{\text{rel}} &= \left(\boldsymbol{T}^{\text{b0}}_T\right)^{-1} \cdot \boldsymbol{T}^{\text{b0}}_B \\ \boldsymbol{T}^{\text{b0}}_{\text{rel}} &= \left(\boldsymbol{T}_T \cdot \boldsymbol{T}_{\text{b0}}\right)^{-1} \cdot \boldsymbol{T}_B \cdot \boldsymbol{T}_{\text{b0}} \\ \boldsymbol{T}^{\text{b0}}_{\text{rel}} &= \boldsymbol{T}_{\text{b0}}^{-1} \cdot \boldsymbol{T}_T^{-1} \cdot \boldsymbol{T}_B \cdot \boldsymbol{T}_{\text{b0}} \end{aligned} \tag{15}$$

$\boldsymbol{T}^{\text{b0}}_{\text{rel}}$ is a 4×4 transformation matrix which can be decomposed into the relative rotation matrix, $\boldsymbol{R}^{\text{b0}}_{\text{rel}}$ (i.e., the rotation component of migration), and relative displacement vector, $\boldsymbol{D}^{\text{b0}}_{\text{rel}}$ (i.e., the displacement component of migration) of the baseplate relative to the tibia.

$$\boldsymbol{T}^{\text{b0}}_{\text{rel}} = \begin{bmatrix} \boldsymbol{R}^{\text{b0}}_{\text{rel}} & \boldsymbol{D}^{\text{b0}}_{\text{rel}} \\ 0^T & 1 \end{bmatrix}$$

$\boldsymbol{R}^{\text{b0}}_{\text{rel}}$ can be further decomposed into θ_x, θ_y, and θ_z using a $x_{GA}y_{GA}z_{GA}$ Cardan angle sequence which is standardized in RSA [4].

Local Baseplate Coordinate System. A local BCS differs from the preceding globally-aligned BCS in that the axes directions and origin are defined by features on the baseplate. To maintain consistency with the ISO standard [5], the local BCS should be defined using anatomic directions (Table 2; Fig. 4). In contrast to the globally-aligned BCS, which places the origin, $\boldsymbol{b}_0$, at the baseplate centroid, we propose to place the origin of the local BCS (still denoted $\boldsymbol{b}_0$) at a point on the lower surface of the tibial tray that is independent of baseplate size which will enhance consistency among several baseplate sizes. For the example baseplate, this point is where the lower surface intersects the central axis of the tibial stem (Fig. 5). Because of the large variation of baseplate designs, the local BCS (i.e., the position of the origin and direction of the three axes) should be clearly described and illustrated.

The local BCS is rotated $\boldsymbol{R}_L$ and displaced $\boldsymbol{D}_L$ in the GCS, where $\boldsymbol{D}_L$ equals $\boldsymbol{b}_0$ (Fig. 6). As performed above, $\boldsymbol{R}_L$ and $\boldsymbol{D}_L$ are combined into a 4×4 transformation matrix $\boldsymbol{T}_L$. The

Table 2 Proposed definitions for the direction of the three axes and position of the origin of the local BCS for a right-sided baseplate

$+y_L$-axis	Perpendicular to the undersurface of the tibial tray pointing proximally
$+z_L$-axis	Perpendicular to the posterior vertical surface of the tibial tray pointing anteriorly
$+x_L$-axis	Cross product of the y_L-axis with the z_L-axis pointing medially
Origin	Point on the lower surface of the tibial tray that is independent of baseplate size. For the example baseplate, this is the point where the lower surface intersects the central axis of the tibial stem (Fig. 5)

transformations of the absolute movements $\boldsymbol{T}_T$ and $\boldsymbol{T}_B$ from the GCS to the local BCS are

$$\boldsymbol{T}_T^L = \boldsymbol{T}_T \cdot \boldsymbol{T}_L \tag{16}$$

$$\boldsymbol{T}_B^L = \boldsymbol{T}_B \cdot \boldsymbol{T}_L \tag{17}$$

For relative movement in the local BCS, substitute Eqs. (16)–(17) into Eq. (12) and simplify

$$\begin{aligned} \boldsymbol{T}_{\text{rel}}^L &= \left(\boldsymbol{T}_T^L\right)^{-1} \cdot \boldsymbol{T}_B^L \\ \boldsymbol{T}_{\text{rel}}^L &= \left(\boldsymbol{T}_T \cdot \boldsymbol{T}_L\right)^{-1} \cdot \boldsymbol{T}_B \cdot \boldsymbol{T}_L \\ \boldsymbol{T}_{\text{rel}}^L &= \boldsymbol{T}_L^{-1} \cdot \boldsymbol{T}_T^{-1} \cdot \boldsymbol{T}_B \cdot \boldsymbol{T}_L \end{aligned} \tag{18}$$

$\boldsymbol{T}_{\text{rel}}^L$, is a 4×4 transformation matrix which can be decomposed into the relative rotation matrix, $\boldsymbol{R}_{\text{rel}}^L$ (i.e., the rotation component of migration) and relative displacement vector, $\boldsymbol{D}_{\text{rel}}^L$ (i.e., the displacement component of migration) of the baseplate relative to the tibia in the local BCS

$$\boldsymbol{T}_{\text{rel}}^L = \begin{bmatrix} \boldsymbol{R}_{\text{rel}}^L & \boldsymbol{D}_{\text{rel}}^L \\ 0^T & 1 \end{bmatrix}$$

$\boldsymbol{R}_{\text{rel}}^L$ can be further decomposed into θ_x^L, θ_y^L, and θ_z^L using a $x_L y_L z_L$ Cardan angle sequence which is standardized in RSA [4].

Clinical Example. Tibial baseplate migration was measured over 1 year in patients who underwent kinematic alignment (KA) TKR [9]. The patient who exhibited the largest magnitude of migration was selected as an example for the present study. Migrations had been previously computed in six degrees of freedom using the local BCS. To demonstrate how deviations in imaging and surgical alignment affect migrations in six degrees of freedom, the migrations using the local BCS were recomputed using a globally-aligned BCS in MATLAB (version R2019a, MATHWORKS, Natick, MA) using clinically relevant rotational deviations (Table 1). To recompute the migrations using the globally-aligned BCS, Eqs. (15) and (18) were rearranged and combined to solve for $\boldsymbol{T}_{\text{rel}}^{b0}$ in terms of $\boldsymbol{T}_{\text{rel}}^L$ as follows:

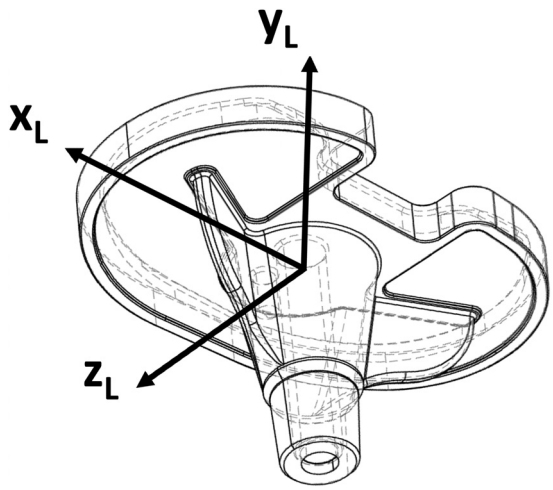

Fig. 4 Proposed local baseplate coordinate system defined by features on the baseplate. The origin location and axes directions are indicated (Table 2).

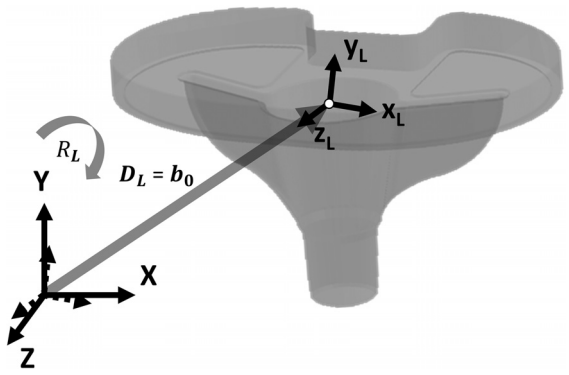

Fig. 6 Illustration of b_0, a vector locating the origin of the local baseplate coordinate system in the global coordinate system. The local baseplate coordinate system is rotated R_L and displaced D_L in the global coordinate system.

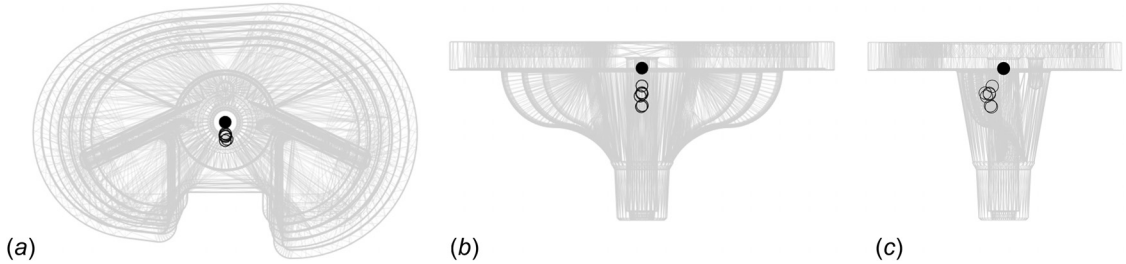

Fig. 5 Overlay of multiple size 3D baseplate models. Views are the (*a*) inferior projection, (*b*) anterior projection, and (*c*) lateral projection. Proposed origin for local BCS is located at the intersection of the center of the stem and the lower surface of the tibial tray and is plotted as a closed black circle (same for all size baseplates). The centroids of the eight baseplate sizes are plotted as open circles showing inconsistency among sizes.

Rearrange Eq. (15)

$$\begin{aligned} \boldsymbol{T}_{\text{rel}}^{\text{b0}} &= \boldsymbol{T}_{\text{b0}}^{-1} \cdot \boldsymbol{T}_{T}^{-1} \cdot \boldsymbol{T}_{B} \cdot \boldsymbol{T}_{\text{b0}} \\ \boldsymbol{T}_{\text{b0}} \cdot \boldsymbol{T}_{\text{rel}}^{\text{b0}} \cdot \boldsymbol{T}_{\text{b0}}^{-1} &= \boldsymbol{T}_{T}^{-1} \cdot \boldsymbol{T}_{B} \end{aligned} \tag{19}$$

Rearrange Eq. (18)

$$\begin{aligned} \boldsymbol{T}_{\text{rel}}^{L} &= \boldsymbol{T}_{L}^{-1} \cdot \boldsymbol{T}_{T}^{-1} \cdot \boldsymbol{T}_{B} \cdot \boldsymbol{T}_{L} \\ \boldsymbol{T}_{L} \cdot \boldsymbol{T}_{\text{rel}}^{L} \cdot \boldsymbol{T}_{L}^{-1} &= \boldsymbol{T}_{T}^{-1} \cdot \boldsymbol{T}_{B} \end{aligned} \tag{20}$$

The rearranged equations now have the same quantities on the right side and can be combined

$$\boldsymbol{T}_{\text{b0}} \cdot \boldsymbol{T}_{\text{rel}}^{\text{b0}} \cdot \boldsymbol{T}_{\text{b0}}^{-1} = \boldsymbol{T}_{L} \cdot \boldsymbol{T}_{\text{rel}}^{L} \cdot \boldsymbol{T}_{L}^{-1}$$

Finally, solve for $\boldsymbol{T}_{\text{rel}}^{\text{b0}}$ in terms of T_{rel}^{L}

$$\boldsymbol{T}_{\text{rel}}^{\text{b0}} = \boldsymbol{T}_{\text{b0}}^{-1} \cdot \boldsymbol{T}_{L} \cdot \boldsymbol{T}_{\text{rel}}^{L} \cdot \boldsymbol{T}_{L}^{-1} \cdot \boldsymbol{T}_{\text{b0}} \tag{21}$$

Differences in migration in six degrees of freedom (globally-aligned BCS migration subtracted from local BCS migration) were plotted against the possible deviations in flexion–extension (FE), internal-external (IE), and varus-valgus (VV) rotations.

Furthermore, because the plots only describe differences with respect to a single rotational deviation (e.g., deviation in FE and no deviation in VV or IE), three examples were presented to show how a combination of rotational deviations affected migration results. One example was for imaging alignment, one was for mechanical alignment (MA), and one was for kinematic alignment (KA). Selected deviations for the imaging alignment example were 20 deg flexion [7], 10 deg internal [6], and 0 deg varus. Selected deviations for the MA example were 5 deg extension [15], 25 deg external [16], and 0 deg varus. Selected deviations for the KA example were 8 deg extension, 9 deg external, and 9 deg varus [9].

Results

For rotational deviations in a single degree of freedom, differences in migration between the two BCSs were largest for rotational deviations in IE and smallest for rotational deviations in VV (Fig. 7). Rotational deviations in FE relative to the imaging plane resulted in differences in migration of about ±0.2 mm in translations and −0.2 deg to 0.3 deg in rotations. Rotational deviations in IE relative to the imaging plane resulted in differences in migration of about ±0.5 mm in translations and −0.4 deg to 0.7 deg in rotations. Rotational deviations in VV relative to the imaging plane resulted in differences in migration of ±0.1 mm in translations and about ±0.1 deg in rotations.

For the three examples, migration values between the globally-aligned BCS and local BCS differed by up to 0.3 mm in translations and 0.4 deg in rotations (Table 3). In the imaging alignment example, the direction of Y translation (i.e., proximal (+) versus distal (−)) was inconsistent between the two coordinate systems. Using the globally-aligned BCS resulted in distal translation (i.e., subsidence) whereas using the local BCS resulted in proximal translation (i.e., liftoff) (Table 3).

Discussion

This paper is the first to describe two conditions—imaging alignment and surgical alignment—which must be satisfied to compute migration relevant to the tibial anatomy and the baseplate-tibia interface, respectively, when using a globally-aligned BCS, and how to implement a local BCS when these conditions are not satisfied. Reasons for using a local BCS, which is defined by features of the 3D baseplate model, were noted in the Introduction: (1) to remove variabilities in imaging alignment (where the patient's anatomy is misaligned with the GCS either accidentally or purposefully to improve registration accuracy [7]) and/or (2) to remove variabilities in surgical alignment (where the baseplate is angled on the tibia). As a result, the local BCS is identical for all patients who receive the same implant, a notable advantage in gaining consistent migration directions between patients while providing clinical relevance.

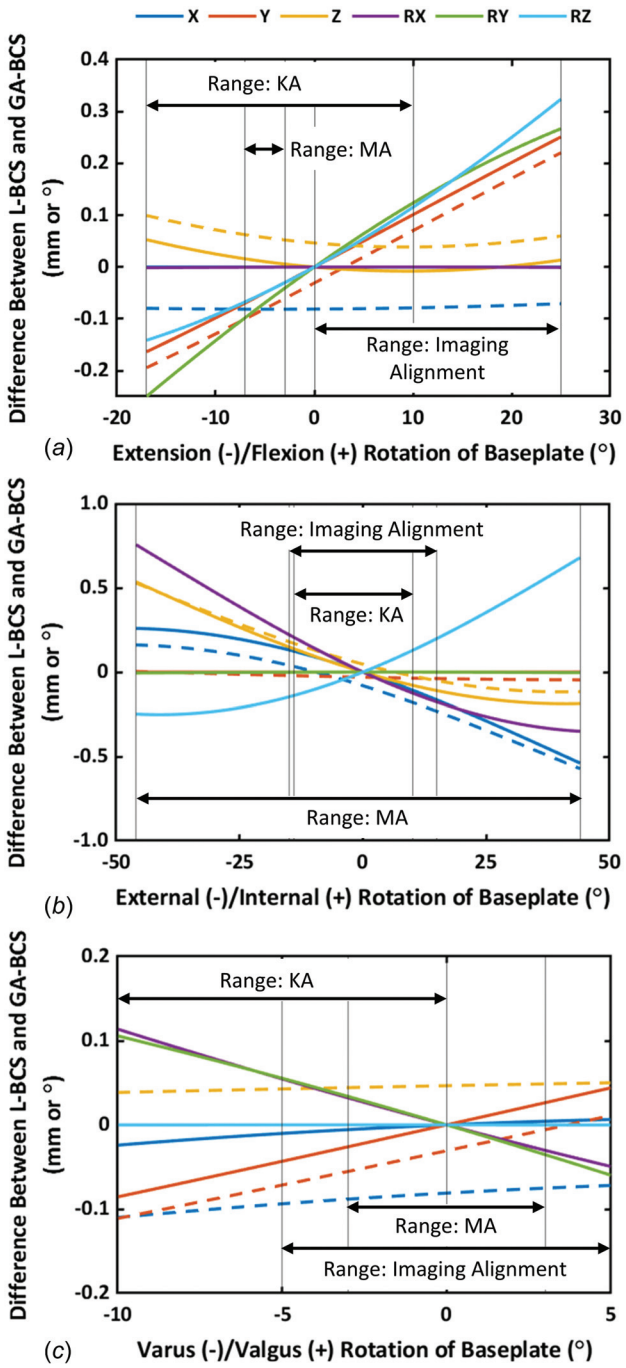

Fig. 7 Plots of the difference in migration in six degrees of freedom for the local BCS (L-BCS) and globally-aligned BCS (GA-BCS) using the example patient migrations transformed for clinically relevant ranges of rotational deviations in (*a*) flexion–extension (FE), (*b*) internal-external (IE), and (*c*) varus-valgus (VV) rotation of baseplate alignment relative to the imaging planes. Solid lines indicate no alteration to the origin's location during the transformation. Dashed lines indicate altering the origin's location during the transformation from that proposed for the local BCS to the centroid for the globally-aligned BCS.

Owing to the variabilities inherent to imaging and surgical alignments, use of the local BCS is advantageous in that the plane formed by the x_L and z_L axes is parallel to the bone resection surface and the y_L-axis is perpendicular to the bone resection surface. This allows direct knowledge of liftoff-subsidence (i.e., y_L-axis translation) of any point located on the baseplate-tibia resection plane, VV rotation (i.e., rotation about the z_L-axis), and FE rotation (i.e., rotation about the x_L-axis) relative to the interface where compromised fixation might occur. Importantly, implementing a local BCS instead of a globally-aligned BCS shifts the definition of the BCS axes from the perspective of the cardinal body planes of the tibia (via the calibration box) to the perspective of the baseplate, and hence the baseplate-tibia interface. Accordingly, the 'anatomic' directions of the local BCS are 'anatomic' relative to the features of the baseplate rather than to the anatomy of the tibia's cardinal body planes per se. As such, RSA researchers can decide which BCS is better suited for their application and/or interests. As noted above, an advantage of the local BCS is its ability to characterize migration relative to the interface where compromised fixation might occur which is arguably of more interest than the alternative.

Recognition of differences in migration between the globally-aligned BCS and local BCS in the clinical examples is important for interpreting the results. Because rotations occurred about more than one axis, migrations in all directions were affected due to kinematic cross-talk (Table 3). Further, although the changes between the globally-aligned BCS and local BCS in an absolute sense were small, nevertheless the relative changes were substantial. In the case of proximal-distal translation, the difference was large enough to cause a sign change for the imaging alignment example. As a result of the sign change, the interpretation of the migration would be affected fundamentally, changing from subsidence in the globally-aligned BCS to liftoff in the local BCS. Hence, this clinical example effectively illustrates the differences between the two BCSs.

To use the local BCS to maximum advantage, some practical issues merit discussion. For baseplate migration with marker-based RSA, the centroid of the baseplate markers is conventionally assigned to be the origin of the globally-aligned BCS [4]. As such, when model-based RSA was developed as a methodology, the centroid of the 3D baseplate model was adopted as the origin [17]. These two points differ since the centroid of the markers depends on their placement. For example, the centroid of markers placed in the polyethylene insert will be more proximal than the centroid of the 3D baseplate model [18]. To remove these variabilities, the authors suggest standardizing the origin of the local BCS across all baseplate designs and multiple implant sizes. The proposed origin is defined as the point where the lower surface of the tibial tray intersects the central axis of the tibial stem (Fig. 5). Although this proposed point differs from convention, it enhances consistency in computed migrations among patients and baseplate designs. Importantly, the choice of the origin will not affect rotations (or the maximum total point motion (MTPM)) only translations (Fig. 7) [19].

Although a notable advantage of using a local BCS is that migrations are independent of patient positioning within the GCS, patient positioning nonetheless merits discussion. Because the bone markers in the tibia serve as a reference for the migration computation, X-ray technicians should still attempt repeatable patient positioning over multiple follow-up examinations such that at least three of the same bone markers are visible in all radiographs. In this case, when acquiring the follow-up radiographs, X-ray technicians should refer to the postoperative reference radiographs at each follow-up examination to obtain similar positioning. To achieve similar positioning, a protocol should be established as to how the patient's anatomy is positioned. For example, to flex the baseplate relative to the imaging planes, the authors use a foam cushion which elevates the patient's knee without elevating the patient's ankle thereby tilting the baseplate anteriorly (Fig. 1(*b*)).

A limitation of the present paper is that the local implant coordinate system was implemented only in the context of tibial baseplate migration for TKR using an example tibial baseplate. When defining a local BCS on any baseplate, the axes directions and

Table 3 Migration values for an example patient using the local BCS and the globally-aligned BCS. Using clinically relevant imaging and surgical alignment deviations, migration values in the local BCS were transformed to those that would have been computed using the globally-aligned BCS. Differences between the two BCSs are shown in parentheses with the Δ symbol.

	Local baseplate coordinate system						
	Translations (mm)			Rotations (°)			
	x_L (+ medial –lateral)	y_L (+ proximal –distal)	z_L (+ anterior –posterior)	x_L (+ flexion –extension)	y_L (+ internal –external)	z_L (+ valgus–varus)	MTPM (mm)
Examples of clinically relevant rotational deviations	−0.5	0.1	0.6	0.7	−0.6	0.8	1.2
	Globally-aligned baseplate coordinate system						
	Translations (mm)			Rotations ( )			
	x_{GA}	y_{GA}	z_{GA}	x_{GA}	y_{GA}	z_{GA}	MTPM (mm)
Imaging alignment: 20 deg flexion, 10 deg internal, 0 deg varus	−0.3 (Δ = +0.2)	−0.1 (Δ = −0.2)	0.6 (Δ = 0.0)	0.8 (Δ = +0.1)	−0.8 (Δ = −0.2)	0.4 (Δ = −0.4)	1.2
Mechanical alignment: 5 deg extension, 25 deg external, 0 deg varus	−0.6 (Δ = −0.1)	0.1 (Δ = 0.0)	0.3 (Δ = −0.3)	0.3 (Δ = −0.4)	−0.5 (Δ = +0.1)	1.0 (Δ = +0.2)	1.2
Kinematic alignment: 8 deg extension, 9 deg external, 9 deg varus	−0.5 (Δ = 0.0)	0.3 (Δ = +0.2)	0.4 (Δ = −0.2)	0.4 (Δ = −0.3)	−0.6 (Δ = 0.0)	0.9 (Δ = +0.1)	1.2

MTPM = maximum total point motion.

origin location should adhere generally to the proposed definitions in Table 2. A local implant coordinate system might be advantageous in other applications such as unicompartmental knee implants, femoral knee implants, and implants in the hip, ankle, or shoulder. For example, when computing migration of the femoral head relative to the femoral shaft after a femoral neck fracture, a recent study aligned the y-axis of the implant coordinate system along the longitudinal axis of the cannulated screw fixing the femoral head to the femoral shaft [20]. Positioning the coordinate system in this manner produced clinically relevant migrations in the context of the fixation device. We limited the scope of this study to include only tibial baseplate migration because there is a large variation in shapes of other implant designs, and it would be impractical to propose a local implant coordinate system for every implant. Importantly, when implementing a local implant coordinate system, the position of the origin and direction of the three axes should be clearly described and illustrated. A final limitation is that the authors recognize that defining a local implant coordinate system is easier to implement in model-based RSA than marker-based RSA because the axes directions and origin location can be defined on the 3D model. Accordingly, using a local implant coordinate system may be less practical for marker-based RSA studies.

Notably, baseplate migration is used to assess the risk of baseplate loosening using stability limits defined in the RSA literature. The most common migration metric used for stability assessment is MTPM. Because MTPM is independent of the coordinate system used to compute migration, when transitioning from using a globally-aligned BCS to a local BCS, the stability limits based on MTPM are unaffected and can be applied. In contrast, another proposed migration metric for assessing baseplate stability is rotation about the transverse axis (i.e., rotation about x_{GA}), where rotation greater than 0.8 deg is considered unstable [21]. Because this stability limit was developed using a globally-aligned BCS to represent baseplate FE, it should be cautiously applied to migrations obtained using a local BCS. In particular, application should be limited to cases in which rotational deviations in VV or IE due to surgical alignment or imaging alignment are small. Fortunately, large rotational deviations in FE do not affect FE migrations (Fig. 7(*a*)). Future proposed stability limits will benefit from using a local BCS because the migrations will be independent of imaging and surgical alignments.

Conclusion

In summary, computing migration consistently among patients and implant designs remains a challenge when using a globally-aligned BCS due to its dependence on the GCS defined by the calibration box. Hence, an alternative approach is to compute migration using a local BCS defined by features on the baseplate. This paper summarized the migration equations for using either the globally-aligned BCS or local BCS, proposed a method for defining a local BCS, and provided clinical examples describing numerical differences. Because migrations computed using a local BCS are independent of imaging and surgical alignments and instead characterize migration using baseplate features, a local BCS enhances consistency in migration directions among patients and baseplate designs relative to the interface in which fixation may be compromised.

Acknowledgment

The authors are grateful to Dr. Petra Heesterbeek and Dr. David Fyhrie for reading the paper and providing recommendations to strengthen it.

Funding Data

- Medacta USA Inc..

Data Availability Statement

The authors attest that all data for this study are included in the paper.

Nomenclature

$\boldsymbol{b}_0$ = vector locating the origin of the baseplate coordinate system. For the globally-aligned baseplate coordinate system, the origin is conventionally the centroid of the baseplate points. For the local baseplate coordinate system, the origin is proposed as a point on the lower surface of the tibial tray that is independent of baseplate size

$\boldsymbol{b}_{\mathrm{fu,i}}$ = vectors representing the location of the baseplate points in the global coordinate system at the follow-up time point

$\boldsymbol{b}_{\mathrm{ref,i}}$ = vectors representing the location of the baseplate points in the global coordinate system at the reference time point

$\boldsymbol{B}_{\mathrm{fu}}$ = matrix of baseplate point vectors in the global coordinate system at the follow-up time point

$\boldsymbol{B}_{\mathrm{ref}}$ = matrix of baseplate point vectors in the global coordinate system at the reference time point

$\boldsymbol{C}$ = an intermediate matrix representing $\boldsymbol{T}_{\mathrm{fu,translated}} \cdot \boldsymbol{T}_{\mathrm{ref,translated}}{}^{T}$

$\boldsymbol{D}_B$ = Displacement vector of $\boldsymbol{B}_{\mathrm{fu}}$ relative to $\boldsymbol{B}_{\mathrm{ref}}$

$\boldsymbol{D}_L$ = displacement vector of the local baseplate coordinate system origin in the global coordinate system; equivalent to $\boldsymbol{b}_0$

$\boldsymbol{D}_{\mathrm{rel}}^{0}$ = displacement vector of $\boldsymbol{B}_{\mathrm{fu}}$ relative to $\boldsymbol{B}_{\mathrm{ref}}$ after registering tibia markers, defined with respect to the origin of the global coordinate system

$\boldsymbol{D}_{\mathrm{rel}}^{L}$ = displacement vector of $\boldsymbol{B}_{\mathrm{fu}}$ relative to $\boldsymbol{B}_{\mathrm{ref}}$ after registering tibia markers, defined with respect to the origin of the local baseplate coordinate system

$\boldsymbol{D}_{\mathrm{rel}}^{b0}$ = displacement vector of $\boldsymbol{B}_{\mathrm{fu}}$ relative to $\boldsymbol{B}_{\mathrm{ref}}$ after registering tibia markers, defined with respect to $\boldsymbol{b}_0$

$\boldsymbol{D}_T$ = displacement vector of $\boldsymbol{T}_{\mathrm{fu}}$ relative to $\boldsymbol{T}_{\mathrm{ref}}$

$\boldsymbol{R}_B$ = rotation matrix of $\boldsymbol{B}_{\mathrm{fu}}$ relative to $\boldsymbol{B}_{\mathrm{ref}}$

$\boldsymbol{R}_L$ = rotation matrix of the local baseplate coordinate system relative to the global coordinate system

$\boldsymbol{R}_{\mathrm{rel}}^{0}$ = rotation matrix of $\boldsymbol{B}_{\mathrm{fu}}$ relative to $\boldsymbol{B}_{\mathrm{ref}}$ after registering tibia markers, defined with respect to the origin of the global coordinate system

$\boldsymbol{R}_{\mathrm{rel}}^{L}$ = rotation matrix of $\boldsymbol{B}_{\mathrm{fu}}$ relative to $\boldsymbol{B}_{\mathrm{ref}}$ after registering tibia markers, defined with respect to the origin of the local baseplate coordinate system

$\boldsymbol{R}_{\mathrm{rel}}^{\mathrm{b0}}$ = rotation matrix of $\boldsymbol{B}_{\mathrm{fu}}$ relative to $\boldsymbol{B}_{\mathrm{ref}}$ after registering tibia markers, defined with respect to $\boldsymbol{b}_0$

$\boldsymbol{R}_T$ = rotation matrix of $\boldsymbol{T}_{\mathrm{fu}}$ relative to $\boldsymbol{T}_{\mathrm{ref}}$

$\boldsymbol{t}_{\mathrm{fu,i}}$ = vectors representing the location of the tibia markers in the global coordinate system at the follow-up time point

$\boldsymbol{t}_{\mathrm{fu,c}}$ = vector representing the location of the centroid of all tibial markers in the global coordinate system at the follow-up time point

$\boldsymbol{t}_{\mathrm{ref,i}}$ = vectors representing the location of the tibia markers in the global coordinate system at the reference time point

$\boldsymbol{t}_{\mathrm{ref,c}}$ = vector representing the location of the centroid of all tibial markers in the global coordinate system at the reference time point

$\boldsymbol{T}_B^L$ = transformation matrix in homogeneous coordinates which combines $\boldsymbol{R}_B$ and $\boldsymbol{D}_B$ then adjusts for rotation and displacement in the local baseplate coordinate system

$\boldsymbol{T}_B^{\mathrm{b0}}$ = transformation matrix in homogeneous coordinates which combines $\boldsymbol{R}_B$ and $\boldsymbol{D}_B$ then adjusts for rotation about $\boldsymbol{b}_0$

$\boldsymbol{T}_T^L$ = transformation matrix in homogeneous coordinates which combines $\boldsymbol{R}_T$ and $\boldsymbol{D}_T$ then adjusts for rotation and displacement in the local baseplate coordinate system

$\boldsymbol{T}_T^{b0}$ = transformation matrix in homogeneous coordinates which combines $\boldsymbol{R}_T$ and $\boldsymbol{D}_T$ then adjusts for rotation about $\boldsymbol{b}_0$

$\boldsymbol{T}_{rel}^0$ = transformation matrix in homogeneous coordinates which describes the relative rotation, $\boldsymbol{R}_{rel}^0$, and relative displacement, $\boldsymbol{D}_{rel}^0$ about the origin of the global coordinate system

$\boldsymbol{T}_{rel}^L$ = transformation matrix in homogeneous coordinates which describes the relative rotation, $\boldsymbol{R}_{rel}^L$, and relative displacement, $\boldsymbol{D}_{rel}^L$ in the local baseplate coordinate system

$\boldsymbol{T}_{rel}^{b0}$ = transformation matrix in homogeneous coordinates which describes the relative rotation, $\boldsymbol{R}_{rel}^{b0}$, and relative displacement, $\boldsymbol{D}_{rel}^{b0}$

$\boldsymbol{T}_{fu,translated}$ = matrix of tibia point vectors in the global coordinate system at the follow-up time point translated such that the centroid is at the origin of the global coordinate system

$\boldsymbol{T}_{fu}$ = matrix of tibia point vectors in the global coordinate system at the follow-up time point

$\boldsymbol{T}_{ref,translated}$ = matrix of tibia point vectors in the global coordinate system at the reference time point translated such that the centroid is at the origin of the global coordinate system

$\boldsymbol{T}_{ref}$ = matrix of tibia point vectors in the global coordinate system at the reference time point

$\boldsymbol{T}_B$ = transformation matrix in homogeneous coordinates which combines $\boldsymbol{R}_B$ and $\boldsymbol{D}_B$

$\boldsymbol{T}_{b0}$ = transformation matrix in homogeneous coordinates composed of the identity rotation matrix (i.e., no rotation) and the displacement vector $\boldsymbol{b}_0$; adjusts for rotation about $\boldsymbol{b}_0$

$\boldsymbol{T}_L$ = transformation matrix in homogeneous coordinates which combines $\boldsymbol{R}_L$ and $\boldsymbol{D}_L$

$\boldsymbol{T}_T$ = transformation matrix in homogeneous coordinates which combines $\boldsymbol{R}_T$ and $\boldsymbol{D}_T$

$\boldsymbol{U}$ = left singular vectors of $\boldsymbol{C}$

$\boldsymbol{V}$ = right singular vectors of $\boldsymbol{C}$

$\boldsymbol{\Sigma}$ = diagonal matrix containing singular values of $\boldsymbol{C}$

Appendix

Migration Equations Using Cartesian Coordinates

Migration Eqs. (12)–(18) presented in the Methods of this paper were written using homogeneous coordinates for mathematical simplicity. For readers who are less familiar with homogeneous coordinates, all of the migration equations using Cartesian coordinates are provided in this Appendix.

Globally-Aligned Baseplate Coordinate System. To compute the relative rotation, the two absolute rotations are combined using Eq. (A1), where the second term is the absolute rotation of the baseplate, and the first term applies the inverse of the absolute rotation of the tibia markers to the absolute rotation of the baseplate

$$\boldsymbol{R}_{rel} = \boldsymbol{R}_T^{-1} \cdot \boldsymbol{R}_B \tag{A1}$$

$\boldsymbol{R}_{rel}$ is decomposed into θ_x, θ_y, and θ_z using a $x_{GA}y_{GA}z_{GA}$ Cardan angle sequence which is standardized in RSA [4]. The Cardan angles θ_x, θ_y, and θ_z define the three rotations of the baseplate (i.e., the rotation component of migration).

An initial transformation is performed to register the tibia markers and remove any difference in patient positioning (i.e., $\boldsymbol{T}_{fu}$ is registered to $\boldsymbol{T}_{ref}$) [11]

$$\boldsymbol{B}_{fu,transformed} = \boldsymbol{R}_T^{-1} \cdot (\boldsymbol{B}_{fu} - \boldsymbol{D}_T \cdot ones) \tag{A2}$$

After the initial transformation, a second transformation is performed to register $\boldsymbol{B}_{fu,transformed}$ to $\boldsymbol{B}_{ref}$. The second transformation describes the migration of the baseplate relative to the tibia which occurs about point, $\boldsymbol{b}_0$, previously described in the main text

$$\boldsymbol{B}_{ref,transformed} = \boldsymbol{R}_{rel} \cdot (\boldsymbol{B}_{ref} - \boldsymbol{b}_0 \cdot ones) + \boldsymbol{b}_0 \cdot ones \tag{A3}$$

Combining Eqs. (A2) and (A3), displacement of the baseplate relative to the tibia simplifies to [11]

$$\begin{aligned} \boldsymbol{D}_{rel}^{b0} &= \boldsymbol{B}_{fu,transformed} - \boldsymbol{B}_{ref,transformed} \\ \boldsymbol{D}_{rel}^{b0} &= \boldsymbol{R}_T^{-1} \cdot (\boldsymbol{B}_{fu} - \boldsymbol{D}_T \cdot ones - \boldsymbol{R}_B(\boldsymbol{B}_{ref} - \boldsymbol{b}_0 \cdot ones)) - \boldsymbol{b}_0 \cdot ones \end{aligned} \tag{A4}$$

Local Baseplate Coordinate System. The baseplate coordinate system is rotated $\boldsymbol{R}_L$ and displaced $\boldsymbol{D}_L$ in the GCS, where $\boldsymbol{D}_L$ equals $\boldsymbol{b}_0$ (Fig. 6). The transformations of the absolute rotations $\boldsymbol{R}_T$ and $\boldsymbol{R}_B$ from the GCS to the local BCS are then

$$\boldsymbol{R}_T^L = \boldsymbol{R}_T \cdot \boldsymbol{R}_L \tag{A5}$$

$$\boldsymbol{R}_B^L = \boldsymbol{R}_B \cdot \boldsymbol{R}_L \tag{A6}$$

For relative rotation in the local BCS, substitute Eqs. (A5)–(A6) into Eq. (A1) and simplify [11]

$$\begin{aligned} \boldsymbol{R}_{rel}^L &= \left(\boldsymbol{R}_T^L\right)^{-1} \cdot \boldsymbol{R}_B^L \\ \boldsymbol{R}_{rel}^L &= (\boldsymbol{R}_T \cdot \boldsymbol{R}_L)^{-1} \cdot \boldsymbol{R}_B \cdot \boldsymbol{R}_L \\ \boldsymbol{R}_{rel}^L &= \boldsymbol{R}_L^{-1} \cdot \boldsymbol{R}_T^{-1} \cdot \boldsymbol{R}_B \cdot \boldsymbol{R}_L \end{aligned} \tag{A7}$$

For relative displacement in the local BCS, first rewrite Eq. (A2) using the local BCS, and simplify [11]

$$\begin{aligned} \boldsymbol{B}_{fu,transformed}^L &= \boldsymbol{R}_L^{-1} \cdot [\boldsymbol{R}_T^{-1} \cdot (\boldsymbol{B}_{fu} - \boldsymbol{D}_T \cdot ones) - \boldsymbol{D}_L \cdot ones] \\ \boldsymbol{B}_{fu,transformed}^L &= \boldsymbol{R}_L^{-1} \cdot \boldsymbol{R}_T^{-1} \cdot (\boldsymbol{B}_{fu} - \boldsymbol{D}_T \cdot ones) - \boldsymbol{R}_L^{-1} \cdot \boldsymbol{D}_L \cdot ones \end{aligned} \tag{A8}$$

Then, rewrite Eq. (A3) using the local BCS (where $\boldsymbol{b}_0$ equals zero) and simplify [11]

$$\begin{aligned} \boldsymbol{B}_{ref,transformed}^L &= \boldsymbol{R}_{rel}^L \cdot \left(\boldsymbol{B}_{ref}^L\right) \\ \boldsymbol{B}_{ref,transformed}^L &= \boldsymbol{R}_L^{-1} \cdot \boldsymbol{R}_T^{-1} \cdot \boldsymbol{R}_B \cdot \boldsymbol{R}_L \cdot \left(\boldsymbol{R}_L^{-1} \cdot (\boldsymbol{B}_{ref} - \boldsymbol{D}_L \cdot ones)\right) \\ \boldsymbol{B}_{ref,transformed}^L &= \boldsymbol{R}_L^{-1} \cdot \boldsymbol{R}_T^{-1} \cdot \boldsymbol{R}_B \cdot (\boldsymbol{B}_{ref} - \boldsymbol{D}_L \cdot ones) \end{aligned} \tag{A9}$$

Last, rewrite Eq. (A4) using the local BCS and simplify [11]

$$\begin{aligned} \boldsymbol{D}_{rel}^L &= \boldsymbol{B}_{fu,transformed}^L - \boldsymbol{B}_{ref,transformed}^L \\ \boldsymbol{D}_{rel}^L &= \boldsymbol{R}_L^{-1} \cdot \boldsymbol{R}_T^{-1} \cdot (\boldsymbol{B}_{fu} - \boldsymbol{D}_T \cdot ones - \boldsymbol{R}_B \cdot \boldsymbol{B}_{ref} \\ &\quad + \boldsymbol{R}_B \cdot \boldsymbol{D}_L \cdot ones) - \boldsymbol{R}_L^{-1} \cdot \boldsymbol{D}_L \cdot ones \end{aligned} \tag{A10}$$

References

[1] Ryd, L., Albrektsson, B. J., Carlsson, L., Dansgard, F., Herberts, P., Lindstrand, A., Regner, L., and Toksvig-Larsen, S., 1995, "Roentgen Stereophotogrammetric Analysis as a Predictor of Mechanical Loosening of Knee Prostheses," J. Bone Jt. Surg. Br., **77-B**(3), pp. 377–383.

[2] Pijls, B. G., Plevier, J. W. M., and Nelissen, R., 2018, "RSA Migration of Total Knee Replacements," Acta Orthop., **89**(3), pp. 320–328.

[3] Pijls, B. G., Valstar, E. R., Nouta, K. A., Plevier, J. W., Fiocco, M., Middeldorp, S., and Nelissen, R. G., 2012, "Early Migration of Tibial Components is

Associated With Late Revision: A Systematic Review and Meta-Analysis of 21,000 Knee Arthroplasties," Acta Orthop., **83**(6), pp. 614–624.
[4] Selvik, G., 1989, "Roentgen Stereophotogrammetry," Acta Orthop Scand, **60**(Suppl. 232), pp. 1–51.
[5] ISO16087:2013(E), 2013, *Implants for Surgery - Roentgen Stereophotogrammetric Analysis for the Assessment of Migration of Orthopaedic Implants*, International Organization for Standardization, Switzerland.
[6] Laende, E. K., Deluzio, K. J., Hennigar, A. W., and Dunbar, M. J., 2009, "Implementation and Validation of an Implant-Based Coordinate System for RSA Migration Calculation," J. Biomech., **42**(14), pp. 2387–2393.
[7] Niesen, A. E., Garverick, A. L., Howell, S. M., and Hull, M. L., 2020, "Reorienting the Tibial Baseplate Improves the Registration Accuracy of Model-Based Radiostereometric Analysis," J. Biomech., **113**, p. 110078.
[8] Lee, Y. S., Howell, S. M., Won, Y. Y., Lee, O. S., Lee, S. H., Vahedi, H., and Teo, S. H., 2017, "Kinematic Alignment is a Possible Alternative to Mechanical Alignment in Total Knee Arthroplasty," Knee Surg. Sports Traumatol. Arthrosc., **25**(11), pp. 3467–3479.
[9] Niesen, A. E., Garverick, A. L., Howell, S. M., and Hull, M. L., 2022, "Low Tibial Baseplate Migration 1 Year After Unrestricted Kinematically Aligned Total Knee Arthroplasty Using a Medial Conforming Implant Design," Knee Surg. Sports Traumatol. Arthrosc., epub.
[10] Nunley, R. M., Nam, D., Johnson, S. R., and Barnes, C. L., 2014, "Extreme Variability in Posterior Slope of the Proximal Tibia: Measurements on 2395 CT Scans of Patients Undergoing UKA?," J. Arthroplasty, **29**(8), pp. 1677–1680.
[11] Leiden University Medical Center Department of Orthopaedics, *Relative Movement Between Objects*, Leiden University Medical Center Department of Orthopaedics, Leiden, The Netherlands, pp. 1–8.
[12] Soderkvist, I., and Wedin, P., 1993, "Determining the Movements of the Skeleton Using Well-Configured Markers," J. Biomech., **26**(12), pp. 1473–1477.
[13] Arun, K., Huang, T., and Blostein, S., 1987, "Least-Squares Fitting of Two 3-D Point Sets," IEEE Trans. Patt. Anal. Mach. Intell., **PAMI-9**(5), pp. 698–700.
[14] Jazar, R. N., 2007, *Theory of Applied Robotics: Kinematics, Dynamics, and Control*, Springer, New York.
[15] Calek, A. K., Hochreiter, B., Hess, S., Amsler, F., Leclerq, V., Hirschmann, M. T., and Behrend, H., 2022, "High Inter- and Intraindividual Differences in Medial and Lateral Posterior Tibial Slope Are Not Reproduced Accurately by Conventional TKA Alignment Techniques," Knee Surg. Sports Traumatol. Arthrosc., **30**(3), pp. 882–889.
[16] Siston, R. A., Goodman, S. B., Patel, J. J., Delp, S. L., and Giori, N. J., 2006, "The High Variability of Tibial Rotational Alignment in Total Knee Arthroplasty," Clin. Orthop. Relat. Res., **452**, pp. 65–69.
[17] Valstar, E. R., Gill, R., Ryd, L., Flivik, G., Borlin, N., and Karrholm, J., 2005, "Guidelines for Standardization of Radiostereometry (RSA) of Implants," Acta Orthop., **76**(4), pp. 563–572.
[18] van Hamersveld, K. T., Marang-van de Mheen, P. J., Koster, L. A., Nelissen, R., Toksvig-Larsen, S., and Kaptein, B. L., 2019, "Marker-Based Versus Model-Based Radiostereometric Analysis of Total Knee Arthroplasty Migration: A Reanalysis With Comparable Mean Outcomes Despite Distinct Types of Measurement Error," Acta Orthop., **90**(4), pp. 366–372.
[19] van Hamersveld, K. T., Marang-van de Mheen, P. J., Tsonaka, R., Nilsson, K. G., Toksvig-Larsen, S., and Nelissen, R., 2021, "Risk Factors for Tibial Component Loosening: A Meta-Analysis of Long-Term Follow-up Radiostereometric Analysis Data," J. Bone Jt. Surg. Am., **103**(12), pp. 1115–1124.
[20] van Embden, D., Stollenwerck, G. A. N. L., Koster, L. A., Kaptein, B., Nelissen, R. G., and Schipper, I. B., 2015, "The Stability of Fixation of Proximal Femoral Fractures," Bone Jt. J., **97-B**, pp. 391–397.
[21] Gudnason, A., Adalberth, G., Nilsson, K. G., and Hailer, N. P., 2017, "Tibial Component Rotation Around the Transverse Axis Measured by Radiostereometry Predicts Aseptic Loosening Better Than Maximal Total Point Motion," Acta Orthop., **88**(3), pp. 282–287.
[22] Nedopil, A. J., Zamora, T., Shelton, T., Howell, S. M., and Hull, M., 2021, "A Best-Fit of an Anatomic Tibial Baseplate Closely Parallels the Flexion-Extension Plane and Covers a High Percentage of the Proximal Tibia," J. Knee Surg., **34**(13), pp. 1486–1494.
[23] Laende, E. K., Richardson, C. G., and Dunbar, M. J., 2019, "A Randomized Controlled Trial of Tibial Component Migration With Kinematic Alignment Using Patient-Specific Instrumentation Versus Mechanical Alignment Using Computer-Assisted Surgery in Total Knee Arthroplasty," Bone Joint J., **101–B**(8), pp. 929–940.